ADVANCES IN OPTICAL POLARIZATION REMOTE SENSING FOR MARINE OBSERVATION: A CASE STUDY IN NANCHANG RIVER PARK

Feizhou Zhang[1], Zihan Zhang[1], Lei Yan[3,1,*], Jing Ding[2,*], Kaiwen Jiang[1], Yulin Zhang[1], Zhiwei Cui[1]

[1] Beijing Key Lab of Spatial Information Integration and 3S Application, Institute of Remote Sensing and Geographic Information System, School of Earth and Space Science, Peking University, Beijing 100871, China
[2] Key Laboratory of Space Ocean Remote Sensing and Application, National Satellite Ocean Application Center, Ministry of Natural Resources, Beijing 100081, China
[3] Guangxi Key Lab of UAV Remote Sensing, Guilin University of Aerospace Technology, Guilin 541004, China

KEY WORDS: Optical polarization remote sensing, Monochrome polarization imaging, Marine observation, Sun-glint observation, Phytoplankton monitoring, Coastal topography mapping.

ABSTRACT:

Marine observation is a worldwide challenge, which implicates for a large number of social, economic and scientific problems. Satellite remote sensing provides incredible convenience for marine observation, and remote sensing techniques with different wavelength range have been developed for scientific use related to oceanography, among of which optical polarization remote sensing is a rapidly growing field in the recent decade. Although some attempts have been made about utilizing optical polarization technique for marine observation, the potential of optical polarization remote sensing is far from being fully released and the current skills of optical polarization image processing are too coarse to extract deep information from raw images. In our experiment at Nanchang river park, three application scenarios are selected to illustrate advances in optical polarization remote sensing for marine observation, specifically including sun-glint observation, phytoplankton monitoring and coastal topography mapping. A baseline for optical polarization image processing is established for marine observation and the advantages of optical polarization technique are assessed qualitatively and quantitatively, proving that: For marine observation, optical polarization remote sensing can reduce overexposure rate, enhance dynamic range, depict subsurface phytoplankton and map coastal topography.

1. INTRODUCTION

To improve our understanding of marine environment and supervision of marine pollution, information detected by marine observation is essential (Garrison, 2012). Sustained observation of global ocean offers broad prospect for ocean parameter retrieval, statistical analysis and marine ecology modelling in support of various oceanography applications (Kennish, 2019).

Satellite remote sensing serves as a powerful means for marine studies on different scales (Emery and Camps, 2017) and in the same time a key to understand the ocean better which accounts for nearly 70% of the Earth surface and comprises 97% of the terrestrial water resources.

Optical polarization remote sensing represents the next generation of remote sensing technique (Yan et al., 2020a) and has been applied in many specific areas of marine observation (e.g., cloud detection (Goloub et al., 2000; Li et al., 2019; Parol et al., 2004), atmospheric correction (Chami et al., 2015; He et al., 2010; Rozanov et al., 2017), aerosol optical depth retrieval (Cheng et al., 2012; Cheng et al., 2011; Gu et al., 2011) and ocean colour retrieval (Chami, 2007; Chami et al., 2001; Wang et al., 2002)). So far, optical polarization remote sensing has not been applied to in-depth studies related to sun-glint observation, phytoplankton monitoring and coastal topography mapping, where polarization optics could be theoretically beneficial.

In this experiment, three specific cases are chosen to illustrate the advances in optical polarization remote sensing for marine observation, and a baseline for optical polarization image processing are utilized to release the potential of optical polarization remote sensing in three different application scenarios including sun-glint observation, phytoplankton monitoring and coastal topography mapping.

2. METHODOLOGY

2.1 Field sites

The study area was located at the central region of Nanchang River Park (39°56′29″N, 116°20′35″E) in Beijing, China. The fieldwork was conducted from 13:00 to 15:00 on October 7th, 2021. A monochrome polarization sensor (LUCID TRI050S-P), ranging from 400 nm – 950 nm, was used for taking polarization image.

2.2 Optical polarization sensor

As for the LUCID TRI050S-P (see Fig. 1(a)), four polarizers (0°, 90°, 45° and 135°, see Fig. 1(b)) are placed on the CMOS (Sony IMX264MZR) for every four pixels (Wen et al., 2021). The spectral response of TRI050S-P with four different directional polarizers is shown in Fig. 1(c). In Fig. 1(c), the black solid line represents the quantum efficiency of the sensor with the polarizer set to 0°, and the red, yellow and blue dashed line represents the difference of quantum efficiency between the 0° polarizer and the 45°, 90° and 135° polarizers respectively. The spectral response difference of this polarization sensor through four directional polarizers are limited within -0.41% – 2.27%, which provides robust optical polarization imaging ability.

* Corresponding author

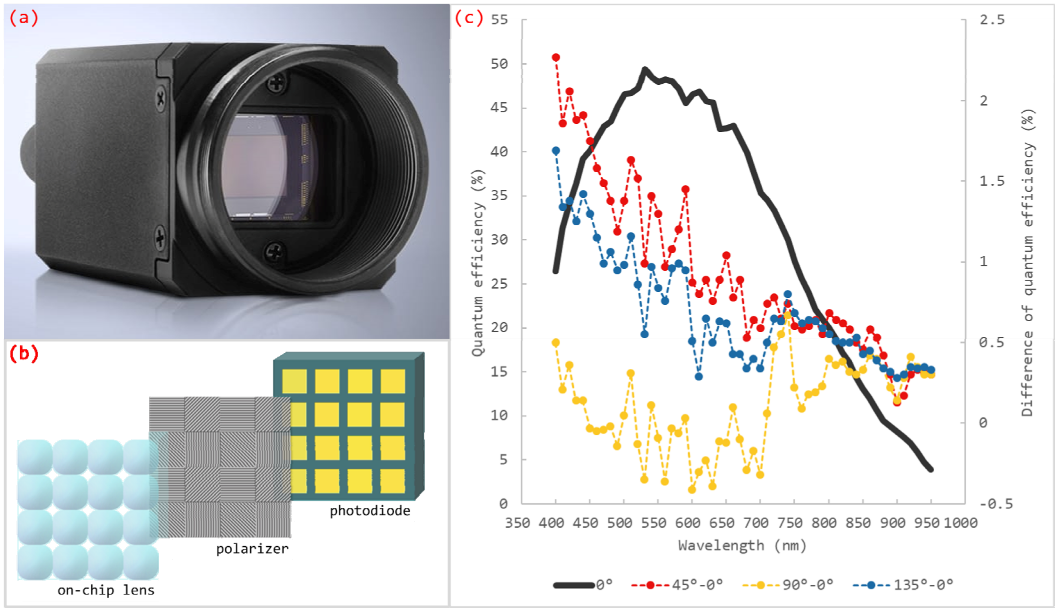

Figure 1. Monochrome polarization sensor (LUCID TRI050S-P)

2.3 Optical polarization model for marine observation

The polarization status S can be described by Stokes vector (Stokes, 1851):

$$S = [I, Q, U, V]^T, \tag{1}$$

where I = the first Stokes parameter, representing the total intensity of the light
Q = the second Stokes parameter, representing the amount of linear horizontal or vertical polarization
U = the third Stokes parameter, representing the amount of linear +45° or -45° polarization
V = the fourth Stokes parameter, representing the amount of right or left circular polarization contained within the beam

Mueller matrix M are used to describe the transition from one polarization status to the other:

$$S' = M \cdot S, \tag{2}$$

where S' = the Stokes vector, representing the polarization status after transition
S = the Stokes vector, representing the polarization status before transition

The Mueller matrix M_θ of an ideal linear polarizer (Yan et al., 2020b) is:

$$M_\theta = \frac{1}{2}\begin{bmatrix} 1 & c & s & 0 \\ c & c^2 & cs & 0 \\ s & cs & s^2 & 0 \\ 0 & 0 & 0 & 0 \end{bmatrix}, \tag{3}$$

where θ = the rotation angle of the polarizer
$c = \cos 2\theta$
$s = \sin 2\theta$

Combining Eq. (2) and Eq. (3), the polarization status $S_\theta = [I_\theta, Q_\theta, U_\theta, V_\theta]^T$ after the light pass through a θ degree polarizer can be calculated:

$$\begin{bmatrix} I_\theta \\ Q_\theta \\ U_\theta \\ V_\theta \end{bmatrix} = \frac{1}{2}\begin{bmatrix} I + cQ + sU \\ cI + c^2Q + csU \\ sI + csQ + s^2U \\ 0 \end{bmatrix}, \tag{4}$$

The polarization sensor directly measures I_θ based on photoelectric response of COMS. Since $I_\theta = I + cQ + sU$, the value of three unknown variables I, Q and U can be calculated by changing the rotation angle θ (implemented with integrated micro-grid polarizers). When the rotation angle is set to 0°, 45°, 90° and 135°, the polarization status of the observed object ($S = [I, Q, U, V]^T$) can be calculated from directional radiation flux $I_{0°}$, $I_{45°}$, $I_{90°}$ and $I_{135°}$:

$$\begin{cases} I = (I_{0°} + I_{45°} + I_{90°} + I_{135°})/2 \\ Q = I_{0°} - I_{90°} \\ U = I_{45°} - I_{135°} \\ V \approx 0 \end{cases}, \tag{5}$$

Combining Eq. (4) and Eq. (5), the radiation flux of a certain rotation angle θ' can be simulated as:

$$\begin{aligned} I_{\theta'} &= \frac{1}{2}(I + c'Q + s'U) \\ &= \frac{1+c'}{2}I_{0°} + \frac{1+s'}{2}I_{45°} + \frac{1-c'}{2}I_{90°} + \frac{1-s'}{2}I_{135°} \end{aligned}, \tag{6}$$

where $c' = \cos 2\theta'$
$s' = \sin 2\theta'$

Degree of polarization DOP and polarization phase angle AOP can be calculated from the polarization status of the observed object ($S = [I, Q, U, V]^T$):

$$DOP = \frac{\sqrt{Q^2 + U^2 + V^2}}{I}, \quad (7)$$

$$AOP = \frac{1}{2}\arctan_2(U, Q), \quad (8)$$

where $\arctan_2$ = four-quadrant arctangent operator

3. RESULTS AND DISCUSSIONS

3.1 Sun-glint observation

Case I is selected to prove the advantage of optical polarization remote sensing in sun-glint observation, and raw polarization images without further image processing are utilized to illustrate the benefits. Since the total intensity decreases (approximately 50%) after the light passes through the polarizer (see Eq. (5)), the polarization sensor provides a wider range of intensity of the incident light and thus suffers less from the problem of overexposure than optical sensor with same CMOS during sun-glint observation. Fig. 2 compares optical intensity image with optical polarization images under sun-glint observation, and the overexposure rates (OER) are listed at the bottom right corner. According to the quantitative comparison, the OER of Fig. 2(a) is the highest, and the OER of all the optical polarization images (Fig. 2(b), Fig. 2(c), Fig. 2(d) and Fig. 2(e)) are significantly lower than that of Fig. 2(a). Qualitatively speaking, Fig. 2(a) is filled with overexposure signals and reveals no practical information. In contrast, the optical polarization images avoid the problem of overexposure to the maximum extent and maintain useful information about subsurface water plants, proving the advantage of optical polarization remote sensing in sun-glint observation.

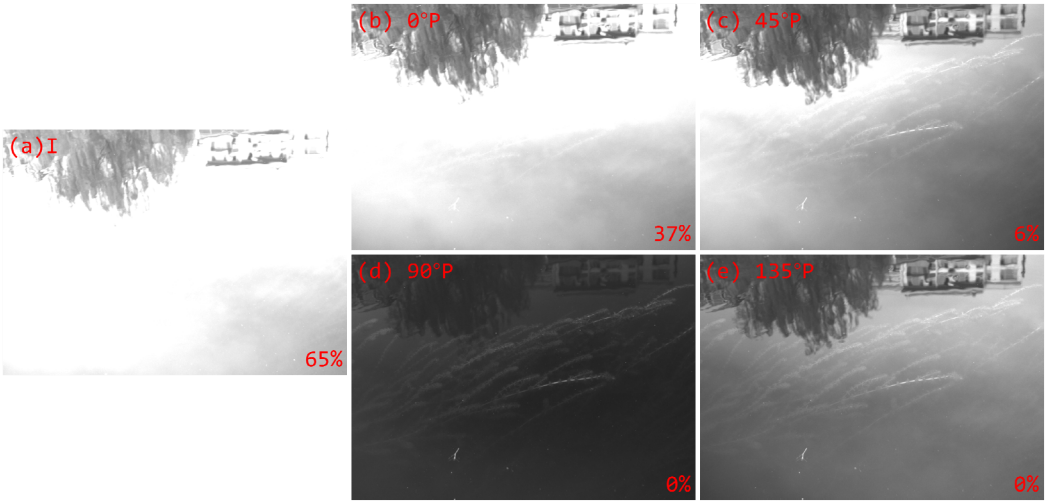

Figure 2. Case I: sun-glint observation

(In Fig. 2, 3 & 4, (a) refers to the optical intensity image; (b), (c), (d) and (e) refers to the raw optical polarization images)

3.2 Phytoplankton monitoring and coastal topography mapping

Case II and case III are selected to illustrate the advantage of optical polarization remote sensing used in phytoplankton monitoring (see Fig. 3) and coastal topography mapping (see Fig. 4), and a baseline for optical polarization image processing based on Eq. (5) and Eq. (6) is established to extract accurate information from the image. The flowchart is shown in Fig. 5.

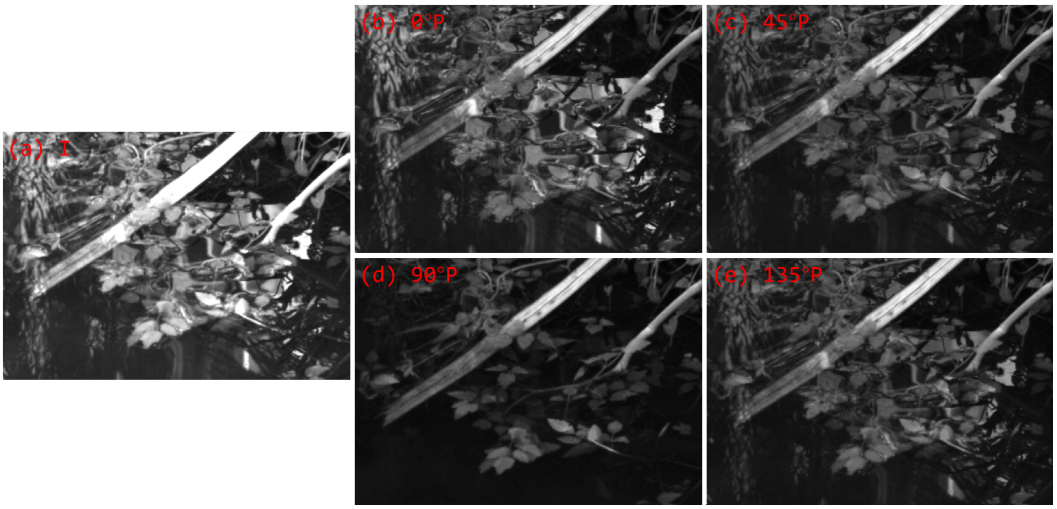

Figure 3. Case II: phytoplankton monitoring

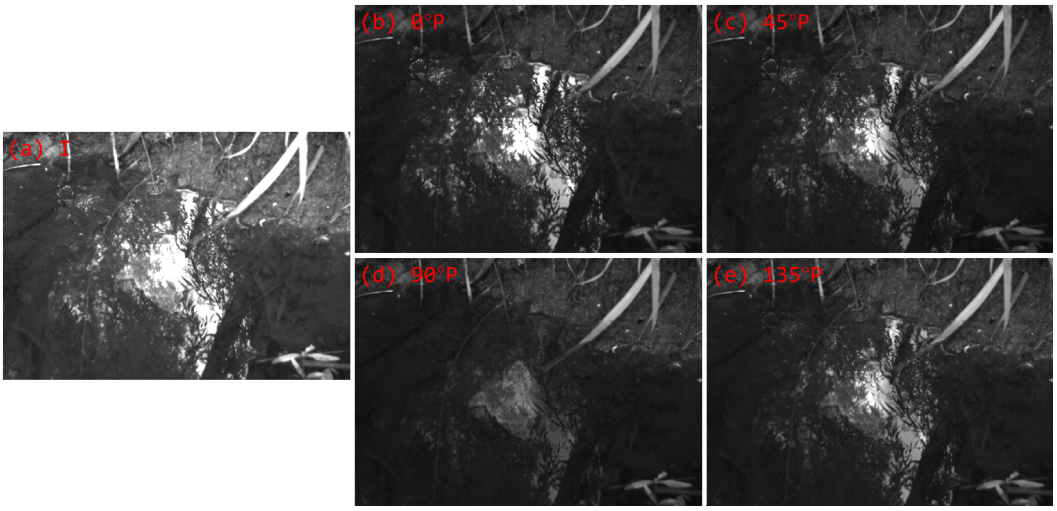

Figure 4. Case III: coastal topography mapping

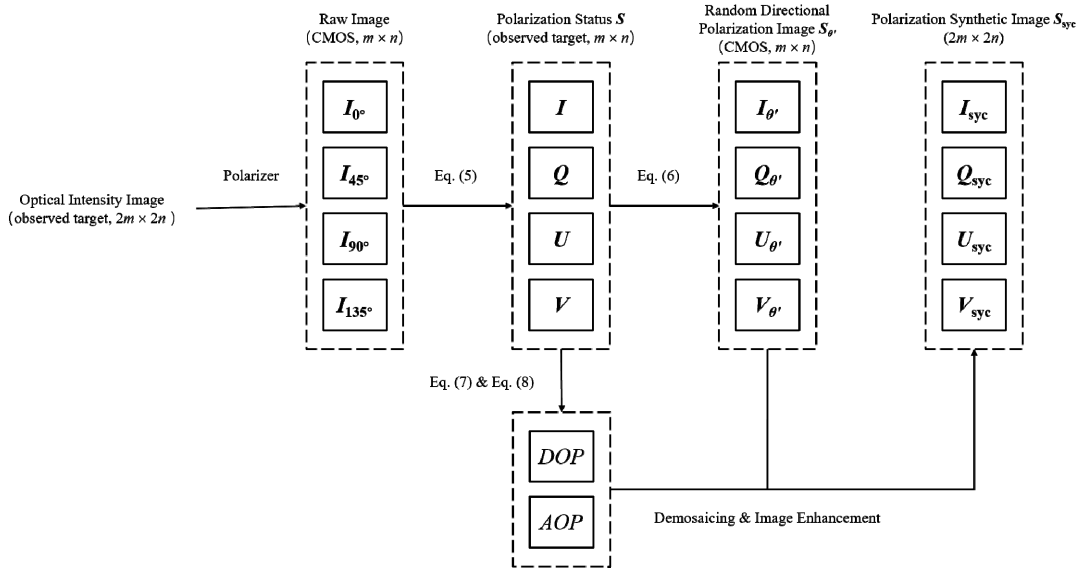

Figure 5. Flowchart of optical polarization image processing

A series of directional polarization images are simulated in order to achieve the best imaging quality (see Fig. 6 and Fig. 7). According to Eq. (6), polarization images with a given rotation angle can be simulated and tested for application, and the simulated directional polarization images are conveniently shown with a 5° interval in Fig. 6 and Fig. 7. Taking recognition rate and contrast ratio as standards, the 97° and 83° optical polarization images are chosen for usage in case II and case III, respectively.

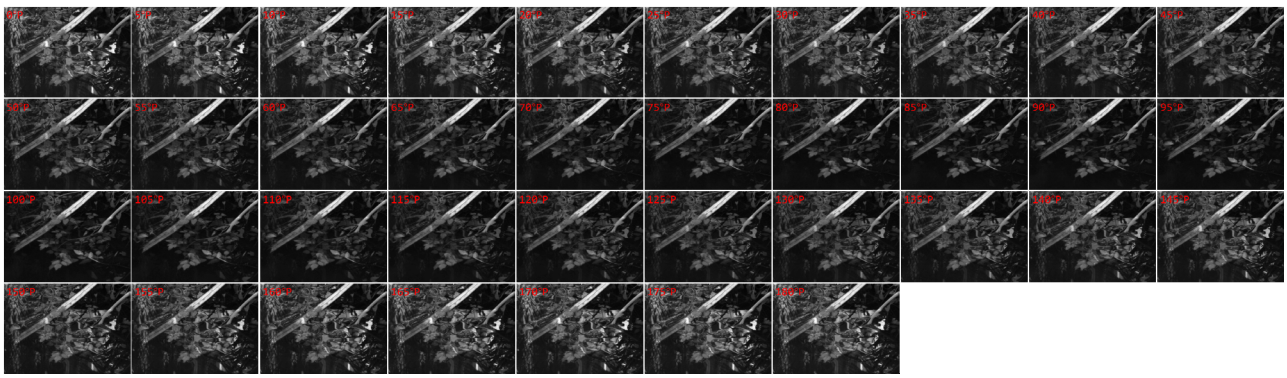

Figure 6. Simulated directional polarization images for case II

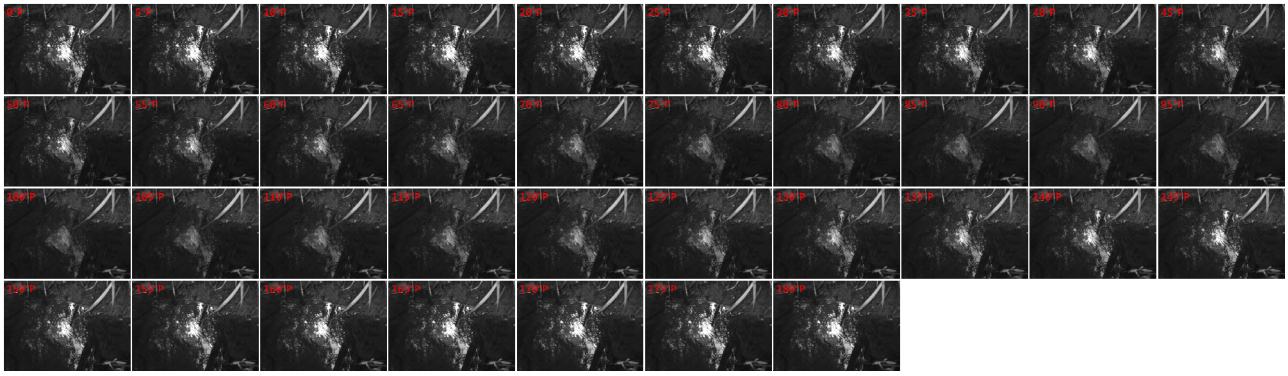

Figure 7. Simulated directional polarization images for case III

After demosaicing by using a pre-trained conditional generative adversarial network (Sargent et al., 2020) based on Eq. (5), the loss of spatial resolution for the directional polarization images is made up and the optical polarization images are rebuilt to the same spatial resolution as the optical intensity images. Then an image enhancement process assisted by *DOP* and *AOP* is used to generate synthetic polarization image. The comparisons between optical intensity images and optical polarization images are shown in Fig. 8 and Fig. 9. In case II, the optical intensity image fails to reveal the sub-surface information, but the optical polarization image successfully pictures the specific outline of sub-surface phytoplankton (see Fig. 8(b)). This case gives an evidence that the distribution and abundance of phytoplankton can be depicted more accurately through optical polarization sensors which can be stably extended to the satellite scale. In case III, the underwater topography can be clearly mapped by optical polarization technique. An eroded rock and topographic relief are shown in Fig. 9(b), indicating that optical polarization remote sensing provides the possibility of mapping coastal topography regardless of tidal ebb and flow, which enables the real-time mapping, change detection and emergency response.

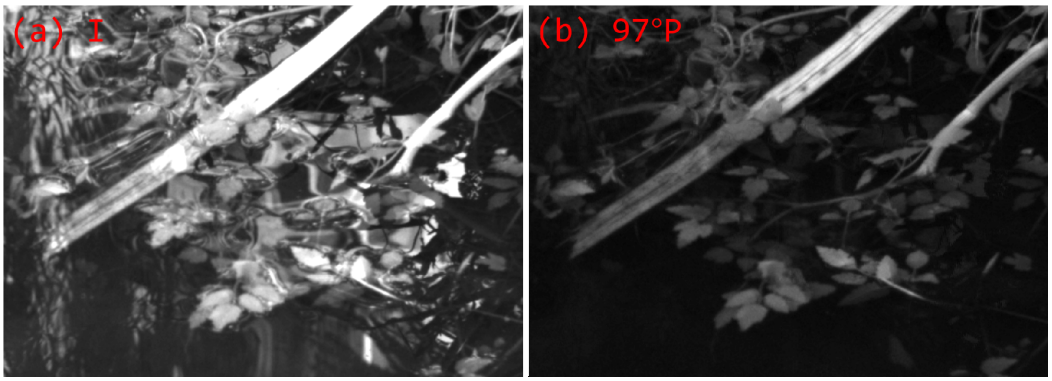

Figure 8. Comparison between optical intensity image and optical polarization image in case II

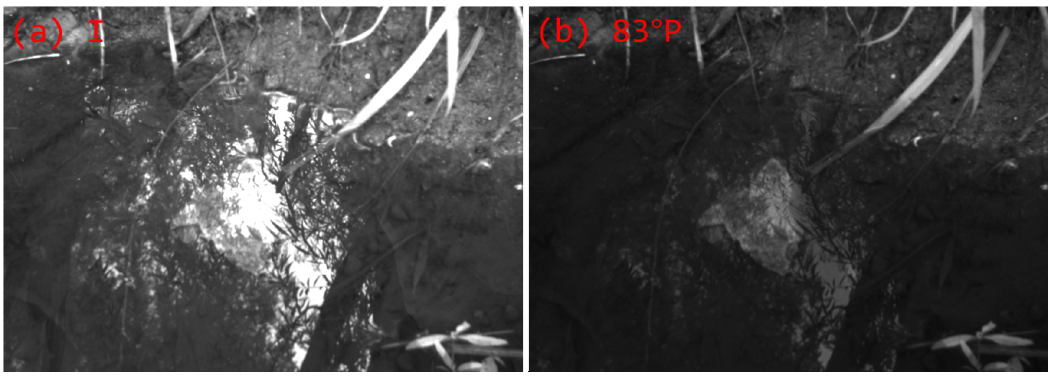

Figure 9. Comparison between optical intensity image and optical polarization image in case III

4. CONCLUSIONS

There are three main contributions in this work: (1) In our ground-based experiment, a baseline of optical polarization image processing is established, which can also be utilized in satellite images. (2) The imaging performance and application effect of optical intensity image and optical polarization image are assessed both qualitatively and quantitatively, proving that optical polarization technique provides many beneficial characteristics in marine observation. (3) The advantages and

potential of optical polarization remote sensing in sun-glint observation, phytoplankton monitoring and coastal topography mapping are carefully discussed, and a roadmap for future adjustment and application is designed.

In the future, with the progress of optical polarization sensor and the development of vector radiative transfer algorithm for coupled atmosphere ocean system, real-time and precise marine observation global network with high spatial resolution would be established, and optical polarization remote sensing would play an increasingly important role in growing kinds of oceanography research areas.

REFERENCES

Chami, M., 2007. Importance of the polarization in the retrieval of oceanic constituents from the remote sensing reflectance. *Journal of Geophysical Research: Oceans*, 112(C5).

Chami, M., Lafrance, B., Fougnie, B., Chowdhary, J., Harmel, T., Waquet, F., 2015. OSOAA: a vector radiative transfer model of coupled atmosphere-ocean system for a rough sea surface application to the estimates of the directional variations of the water leaving reflectance to better process multi-angular satellite sensors data over the ocean. *Optics Express*, 23(21), 27829-27852.

Chami, M., Santer, R., Dilligeard, E., 2001. Radiative transfer model for the computation of radiance and polarization in an ocean–atmosphere system: polarization properties of suspended matter for remote sensing. *Applied Optics*, 40(15), 2398-2416.

Cheng, T., Gu, X., Xie, D., Li, Z., Yu, T., Chen, H., 2012. Aerosol optical depth and fine-mode fraction retrieval over East Asia using multi-angular total and polarized remote sensing. *Atmospheric Measurement Techniques*, 5(3), 501-516.

Cheng, T., Gu, X., Xie, D., Li, Z., Yu, T., Chen, X., 2011. Simultaneous retrieval of aerosol optical properties over the Pearl River Delta, China using multi-angular, multi-spectral, and polarized measurements. *Remote Sensing of Environment*, 115(7), 1643-1652.

Emery, B., Camps, A., 2017. *Introduction to satellite remote sensing: atmosphere, ocean, land and cryosphere applications*. Elsevier.

Garrison, T.S., 2012. *Oceanography: an invitation to marine science*. Cengage Learning.

Goloub, P., Herman, M., Chepfer, H., Riédi, J., Brogniez, G., Couvert, P., Sèze, G., 2000. Cloud thermodynamical phase classification from the POLDER spaceborne instrument. *Journal of Geophysical Research: Atmospheres*, 105(D11), 14747-14759.

Gu, X., Cheng, T., Xie, D., Li, Z., Yu, T., Chen, H., 2011. Analysis of surface and aerosol polarized reflectance for aerosol retrievals from polarized remote sensing in PRD urban region. *Atmospheric Environment*, 45(36), 6607-6612.

He, X., Bai, Y., Zhu, Q., Gong, F., 2010. A vector radiative transfer model of coupled ocean–atmosphere system using matrix-operator method for rough sea-surface. *Journal of Quantitative Spectroscopy and Radiative Transfer*, 111(10), 1426-1448.

Kennish, M.J., 2019. *Practical handbook of marine science*. CRC Press.

Li, C., Ma, J., Yang, P., Li, Z., 2019. Detection of cloud cover using dynamic thresholds and radiative transfer models from the polarization satellite image. *Journal of Quantitative Spectroscopy and Radiative Transfer*, 222, 196-214.

Parol, F., Buriez, J.-C., Vanbauce, C., Riédi, J., Doutriaux-Boucher, M., Vesperini, M., Sèze, G., Couvert, P., Viollier, M., Bréon, F., 2004. Review of capabilities of multi-angle and polarization cloud measurements from POLDER. *Advances in Space Research*, 33(7), 1080-1088.

Rozanov, V., Dinter, T., Rozanov, A., Wolanin, A., Bracher, A., Burrows, J., 2017. Radiative transfer modeling through terrestrial atmosphere and ocean accounting for inelastic processes: Software package SCIATRAN. *Journal of Quantitative Spectroscopy and Radiative Transfer*, 194, 65-85.

Sargent, G.C., Ratliff, B.M., Asari, V.K., 2020. Conditional generative adversarial network demosaicing strategy for division of focal plane polarimeters. *Optics Express*, 28(25), 38419-38443.

Stokes, G.G., 1851. On the composition and resolution of streams of polarized light from different sources. *Transactions of the Cambridge Philosophical Society*, 9, 399.

Wang, M., Isaacman, A., Franz, B.A., McClain, C.R., 2002. Ocean-color optical property data derived from the Japanese Ocean Color and Temperature Scanner and the French Polarization and Directionality of the Earth's Reflectances: a comparison study. *Applied Optics*, 41(6), 974-990.

Wen, S., Zheng, Y., Lu, F., 2021. A Sparse Representation Based Joint Demosaicing Method for Single-Chip Polarized Color Sensor. *IEEE Transactions on Image Processing*, 30, 4171-4182.

Yan, L., Li, Y., Chandrasekar, V., Mortimer, H., Peltoniemi, J., Lin, Y., 2020a. General review of optical polarization remote sensing. *International Journal of Remote Sensing*, 41(13), 4853-4864.

Yan, L., Yang, B., Zhang, F., Xiang, Y., Chen, W., 2020b. *Polarization Remote Sensing Physics*. Springer Nature.